Optical Fibre Humidity Sensors Using Nano-films

Jesus M. Corres, Ignacio R. Matias and Francisco J. Arregui

Abstract This chapter attempts to approach the fibre optic humidity sensing technology to scientists unfamiliar with the field. A general review of this type of sensors is presented here with emphasis in the techniques based on nanostructured coatings. These devices have been classified according to the sensing mechanism and taking also into account the different methods of fabrication and the sensing materials they are based on.

Keywords Optical fibre sensor · humidity sensor · humidity sensitive nano-films

1 Introduction

The monitoring of humidity is a necessary activity in numerous fields of industry because it may affect both the product, and the health and security of the workers; for instance humidity measurement can be of vital importance in chemical and biomedical industries. Also, humidity sensing is frequently monitored in big structures such as bridges or planes to control possible risk of leakage due to corrosion [1, 2]. Therefore relative humidity measurement has been extensively studied and a great variety of sensors, including capacitive, resistive, thermal conductivity and optical have been developed along the last decades.

So far, electronic humidity sensors cover the main part of the sensors market because their technology of fabrication is very established. However, the field of

Jesus M. Corres
Departamento de Ingeniería Eléctrica y Electrónica, Universidad Pública de Navarra, Pamplona, Spain, e-mail: jmcorres@unavarra.es

Ignacio R. Matias
Departamento de Ingeniería Eléctrica y Electrónica, Universidad Pública de Navarra. Pamplona, Spain

Francisco J. Arregui
Departamento de Ingeniería Eléctrica y Electrónica, Universidad Pública de Navarra. Pamplona, Spain

S.C. Mukhopadhyay, R.Y.M. Huang (eds.), *Sensors*,

optical fibre sensors has grown enormously since the 60's and at the present time there exist niches of application where optical fibre humidity sensor technology can advantageously compete with traditional (mainly electronics) technologies.

Fibre optic humidity sensors (FOHS) use optical fibre technology to guide a light signal which is modulated with the ambient humidity and then collected back by a detector, conditioned and processed. Thanks to the low attenuation and large wideband of fibre it is possible to transmit large sensor data quantities over kilometre distances; in addition, the use of several interrogating techniques enable the existence of distributed humidity sensors configurations [3]. There are also a high number of applications where the possible electric hazard produced by the electronic sensor itself or the electromagnetic interferences of the surrounding environment makes difficult the utilization of electronic type humidity sensors. In some fields it is needed a measurement of humidity where the accessibility is limited in space and an electronic sensor could be more difficult to locate. The small dimensions and simple geometries of optical fibre make possible the implementation of light-weight systems that can be easily embedded into construction materials. Finally, the sensitivity, dynamic range and resolution can be potentially much greater than conventional sensors with the use of interferometric techniques.

A number of different approaches have been used in the fabrication of optical fibre humidity sensors. Fibre optic sensors are commonly subdivided into intrinsic (if the transduction between the light and the measurand takes place inside the fibre) and extrinsic (if it takes place outside it). In practice, most of humidity sensors are of extrinsic type because the fibre is immune to humidity, with the exception of special fibres fabricated using porous materials such as sol gel. Depending on the sensing architecture, transmissive and reflexive humidity sensors can be found and more subdivisions are possible depending on the sensing mechanism.

In this chapter, a summary of the most representative architectures for the construction of optical fibre humidity sensors based on nano-films will be presented. Due to the complexity of this field, this text will try to approach the FOHS to engineers and scientists unfamiliar with the field. Classical architectures will be presented here as well as the state of art related to FOHS. Prior to this, an introduction to the sensitive materials and deposition techniques that are usually employed in the fabrication of these sensors will be described next. Among these techniques, nanotechnology has recently emerged as a new and challenging discipline where the scientific community is being greatly involved. One of the more promising techniques included in the commonly called 'botton-up nanotechnology' is the LbL technique. As this one can summarize by itself the different fibre optic sensing architectures using sensitive nano-films, this chapter will be mainly focused on the LbL technique. Furthermore, since its rediscovery in the nineties, the layer-by-layer (LBL) self-assembly has found a great acceptance between the optical fibre sensor community.

2 Humidity Sensing Materials and Deposition Techniques

Direct detection of water vapour is possible without the use of any sensing material, for instance with the employ of specialised optics to determine the refractive index of air [4] or the air density changes [5]. However these techniques require the use of expensive systems such as radioactive alpha-ray sources.

Otherwise, relative humidity (RH) can be measured through the properties of some bulk material such as the change in either its physical dimensions or refractive index. Because of that, the vast majority of FOHS developed require the presence of a sensing film whose properties change as a function of the ambient humidity. In addition to this, the material should readily absorb and desorb water.

Both organic and inorganic polymers are used for optical sensors fabrication including silicones, PVC, PTFE, PMMA, nafion, nylon, agarose, sol-gels, etc. [6, 7, 8]. These materials usually give good robustness to the sensor design. The humidity sensing can be achieved by the incorporation of a reagent or by the polymer structure itself. The reagent is a dye which reversibly changes its optical properties with the humidity. Several humidity sensors have been reported based on such well-known reagents. Ideally the wavelengths used for detecting the changes are in the visible or near-infrared region which permits the use of low cost instrumentation and standard fibres. This change is marked in complexes of transition metals. $CoCl_2$ is one of the most commonly used materials for this purpose because it can absorb water and form coordination complexes which change its characteristic colour [9, 10, 11, 12, 13]. When dry, it has strong absorption in the wavelength range 550–700 nm showing a blue colour, while it does not absorbs when it gets wet (forming an hexa-hydrated compound) which results in a pink colour. Other type of humidity sensors are those based on fluorescent and phosphorescent materials such as rhodamine [14, 15] or AI-Ferron [16]. The main advantage of these sensors is that lifetime based measurement can be used, which does not depend on the light-source intensity changes caused by the sensing molecule, the transducer, or the optical path [16]. However, these types of sensors have an important cross sensitivity with temperature.

On the other hand, instead of using a reagent, another different strategy consists of using hygroscopic polymers which, as a general rule, swell when water enters the structure. Hydrophilic gels, such as agarose [17], have a high porosity which determines the quantity of water that the gel is capable of absorbing and therefore its performance as working as humidity sensor. When the water content increases, it induces the gel film to swell which generates a reduction in the refractive index. High refractive index materials increase the interaction between the light guided in the fibre and the sensitive film and hence it increases the sensitivity of the sensor; for instance, PMMA has been used for humidity sensing [6, 18] reporting fast response times (5 s) operating in the range 20–80% RH with complete reversibility.

Among the deposition techniques, it could be said that the classical ones, such as physical vapor deposition or spin coating are intended usually for flat semiconductor substrates and cannot deposit easily uniform films on complex geometries, like

in optical fibres. Actually, to our knowledge, there are three techniques that have been successfully used for the deposition of uniform coatings onto optical fibres such as the dip-coating (DC) technique, the Langmuir-Blodgett (LB) technique and the layer-by-layer (LbL) technique. The first one is usually associated to sol-gel or hydrogel coatings, but it is not useful for controlling the thickness of the coatings on the nanometer scale. In contrast to this, using the former techniques it is possible to deposit coatings of specific nanometer thickness.

2.1 Nanostructured Films

A recently open line of research of suitable humidity materials is focused on nanostructured materials. The use of these materials confers several advantages for humidity sensing like shorter response times and enhanced sensitivity [19, 20, 21, 22, 23, 24, 25]. These fibre optic sensors are based on the deposition of a controlled thickness layer onto the surface of the fibre. The light passing through the fibre is modulated by the thin layer whose refractive index changes as a function of the external relative humidity [26]. As it has been previously commented, the LB and LbL techniques can be used for the fabrication of nanostructured films controlling the thickness of the coatings on the nanometer scale. The LbL process has been successfully proved as a useful tool for the fabrication of nanostructured materials that include many diverse species, such as colorimetric dyes, fluorescent indicators, inorganic semiconductors, conducting polymers, ceramics, metals, quantum dots, enzymes, antibodies or even DNA strands.

The use of nanometric scale films enable the fabrication of sensor heads based on nano-films in which the humidity easily interacts with the film and provoke changes in the entire effective detection zone. In particular, using one of these techniques, speeds of response below 1s have been reported [19].

Layer by layer process was reported for the first time by R. Iler [27] and almost thirty years later the technique was rediscovered by G. Decher and co-workers [28], and extended to the layering of polyelectrolytes and many other systems [29, 30, 31, 32, 33, 34, 35, 36, 37, 38, 39, 40, 41, 42, 43, 44, 45, 46]. In the last seven years the number of works on this topic has increased exponentially and some reviews permit to understand the current state of the art [47, 48, 49, 50, 51, 52]. The versatility of LBL method for the synthesis of materials permits the application of this technique to design or fabrication of different structures on the tip or the cladding of the optical fibre.

The deposition procedure for all cases is based on the construction of molecular multilayers by the electrostatic attraction between oppositely charged polyelectrolytes in each monolayer deposited, and involves several steps. The LbL film deposition method is schematically depicted in Fig. 1.

First, a substrate is cleaned and treated to create a charged surface. Then, the substrate is exposed to a solution of a polyion of opposite charge for a short time (minutes) and, by adsorption, a monolayer of polyions is formed on the surface.

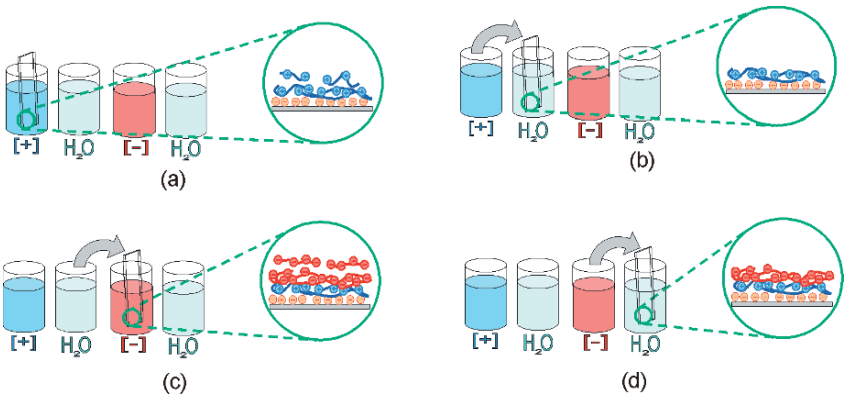

Fig. 1 Schematic representation of the LbL method. (**a**) Adsorption of a cationic monolayer and inversion of the surface charge. (**b**) Washing with ultrapure water. (**c**) Adsorption of anionic monolayer. (**d**) Washing with ultrapure water

Subsequently, the substrate is alternately dipped into solutions of cationic and anionic polymers (or appropriately charged inorganic clusters) to create a multilayer thin film, a polyanion-polycation multilayer. After each monolayer is formed, the sample is rinsed in pure water to remove the excess of molecules that are not bound and that do not contribute to the monolayer structure.

The molecular species of the cationic and anionic components and the long-range physical order of the layers determine the resulting coating properties. It is important to notice that the polyanions and polycations overlap each other at the molecular level and this produces an optically homogeneous material.

The individual layer composition and thickness can be controlled with different parameters. The most important ones are the temperature, the pH and the concentration of the solutions, the dipping time, the drying time and the substrate where the structure is being deposited. Typical individual layer thickness values range between 0.5 and 15 nm [53]. However, it has been studied with other materials that the range can be widened to 60 nm [54].

An interesting property from the point of view of humidity sensor design is the hydrophobicity and hydrophilicity of the films. If adequately designed, the film can be used for the fabrication of sensors with fast response and low hysteresys.

In addition, other deposition procedures are available; this is the case of the above commented Langmuir-Blodgett technique. This method is based on the deposition of layers with hydrophobic and hydrophilic behavior [55, 56]. Each bilayer to be deposited is spread onto ultrapure water, forming a nanometric surface; when the substrate, in this case the optical fibre, is introduced in the solution, a new layer gets deposited onto the surface [57]. Unfortunately, the LB technique is limited to very specific molecules with combinations of lipophilic and hydrophilic parts.

In any case, most of the sensors based on sensitive nanocoatings, deposited either using sol-gel, LB or LbL techniques, are evanescent wave based sensors. An evanescent wave is a standing harmonic wave located at the core/cladding interface.

This wave penetrates over a small distance (typically below one micron) into the surrounding medium. The evanescent wave and can be described by the exponential decay [58].

$$E = E_o \exp(-z/d_p) \tag{1}$$

where z is the distance normal to the interface and E_o is the wave amplitude at $z = 0$.

The penetration depth is given by

$$dp = \frac{\lambda}{2\pi n_1} \sqrt{\sin^2\theta - (n_2/n_1)^2} \tag{2}$$

where λ is the wavelength of the light in the fibre core, n_l and n_2 are the refractive indices of the core and cladding materials, respectively, and θ is angle of incidence. The thinner is the coating, on the order of the penetration depth, the faster and more efficient its reaction will be.

3 Optical Techniques Used In Fibre Optic Humidity Sensors

Basically, any optical fibre sensor can be classified into a reflexive or transmissive structure. In a reflection-type configuration, the sensing material is located at the end point of the fibre, being especially adequate for applications where the sensor head dimension is important, because it can be easily miniaturized and handled.

In general a higher sensitivity can be obtained with the use of a transmissive configuration. A more important part of the guided power, with respect to the reflective configuration, enters in contact with the sensing film and is modulated and transmitted by the output fibre. There are many possible implementations of evanescent wave sensors. There not exist also other architectures based on wavelength or phase changes, but are no so popular.

3.1 Reflective Sensors Based on Coating Deposition on the Tip of the Fibre

In this scheme, the incident light travels along one optical fibre and illuminates the humidity sensing material. The light reflected or emitted in this case is collected back and transmitted along the same fibre. The sensor head consists of a cleaved or polished end of an optical fibre, onto which the humidity sensitive material is deposited.

In Fig. 2 it is represented the scheme of a fibre tip coated using the LbL method. The thickness of the interferometric cavity increases as the number of adsorbed layers is higher. The refractive index of the film (n_2) can be higher or lower than the fibre (n_1). For example, the nanostructured material [PDDA/PolyR] gives refractive

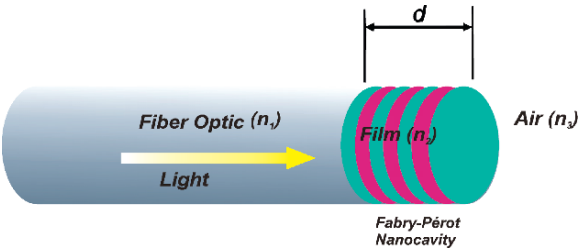

(a)

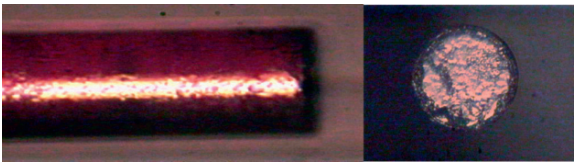

(b)

Fig. 2 (**a**) Coating deposition on the tip of the fibre forming a nanoFabry-Pérot cavity (**b**) Photograph of a fibre tip humidity sensor

indexes higher than that of the fibre (1.55–1.60), while other porous films based on SiO_2 nanoparticles gives values of n_2 around 1.2–1.25.

The reflected power when n_2 is higher than n_1 is given by [60],

$$R_{FP} = \frac{I_R}{I_0} = \frac{R_1 + R_2 \cdot (1 - A_1)^2 \cdot e^{-\alpha \cdot 4d} + 2 \cdot \sqrt{R_1 \cdot R_2} \cdot (1 - A_1) \cdot e^{-\alpha \cdot 2d} \cdot \cos\phi}{1 + R_1 \cdot R_2 \cdot e^{-\alpha \cdot 4d} + 2 \cdot \sqrt{R_1 \cdot R_2} \cdot e^{-\alpha \cdot 2d} \cdot \cos\phi} \tag{3}$$

where ϕ is the round-trip phase shift of the optical beam in the cavity formed by the coating with thickness d, and R_1 is the reflection coefficient at the first interface (optical fibre–coating) and R_2 is the reflection coefficient at the second interface (coating–air), α is the absorption coefficient of the coating and A_i is a factor associated to the scattering losses.

The following expression permits to estimate the thickness of each nanocavity bilayer [59, 60]:

$$\phi = \frac{4 n_2 d \pi}{\lambda} \tag{4}$$

where n_2 is the real refractive index of the coating, and λ is the wavelength of the LED. The destructive interference occurs when ϕ is an odd multiple of π, which indicates that it appears for a lower length d.

As can be seen in Fig. 3, the light is coupled from the source and is guided until the sensor head, where the light interacts with the humidity sensing material. The reflected signal from the sensitive film is transmitted to the optical detector. To achieve this, an optical coupler is necessary to drive the response signal to the detection system. Since the cavity created at the end of fibre is much shorter than the coherence length of a LED source, this permits to avoid the necessity of an expensive laser device to monitor interferometric phenomenon caused by changes in the refractive index of the material deposited.

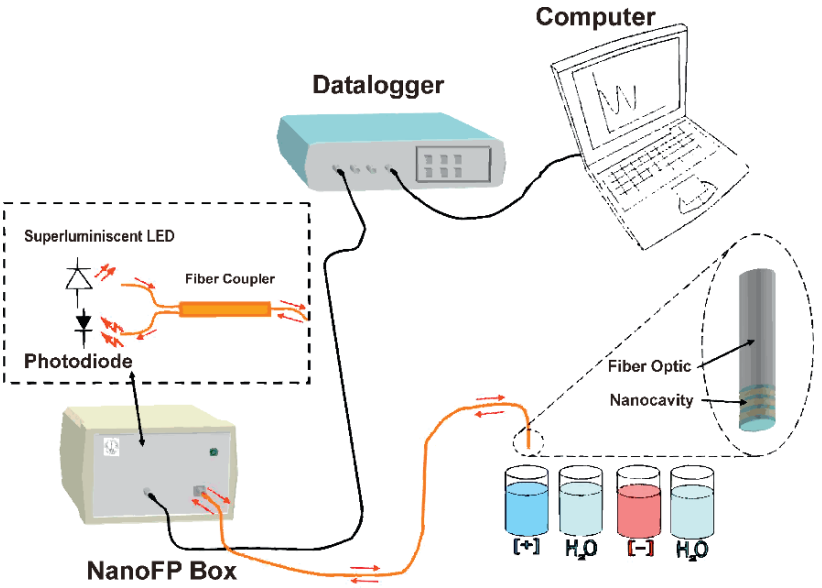

Fig. 3 Experimental set-up used for monitoring the reflected optical power during the LBL process deposition at the end of the fibre. The same scheme is used for humidity monitoring

In addition to the measurement of the target parameter by means of the variation of the output optical power, it is also important to note that with the same scheme it is possible to monitor the power fluctuations during the building of the nanocavity. As most of the materials deposited in the nanocavity are highly lossy, the reflected power changes with a sinusoidal shape during the construction process, which is caused by the light interference in two beams nanoFabry-Pérot (or Fizeau) cavity. Using an optimization algorithm it is possible to estimate the film growing ratio each layer is deposited.

In [60] this scheme was used to measure RH using a solution of poly (diallydimethyl ammonium chloride) (PDDA) as the cation solution and the molecular dye PSS for the anionic solution. The combination of PDDA+ and PSS- was deposited onto the sensor head using the LbL technique, creating a nanoFabry-Pérot cavity which attracts water molecules. Consequently, the thickness of the device is a function of the humidity. As the refractive index and the thickness of the nanocavity get modified by the environmental humidity, there is a change in the reflected optical power detected. The response time is so fast that these sensors can be used even for human breathing monitoring [60], as can be seen in Fig. 4. In addition, the sensors showed a repetitive response.

In [61] the same structure was used, but changing the coating by a super hydrophilic nano-film based on SiO_2 nanoparticles, and thus highly sensitive to humidity.

The response time of a fibre optic humidity sensor based on SiO_2 nanoparticles [61] is shown in Fig. 5. In this case, the rise and fall times are only 150 ms and

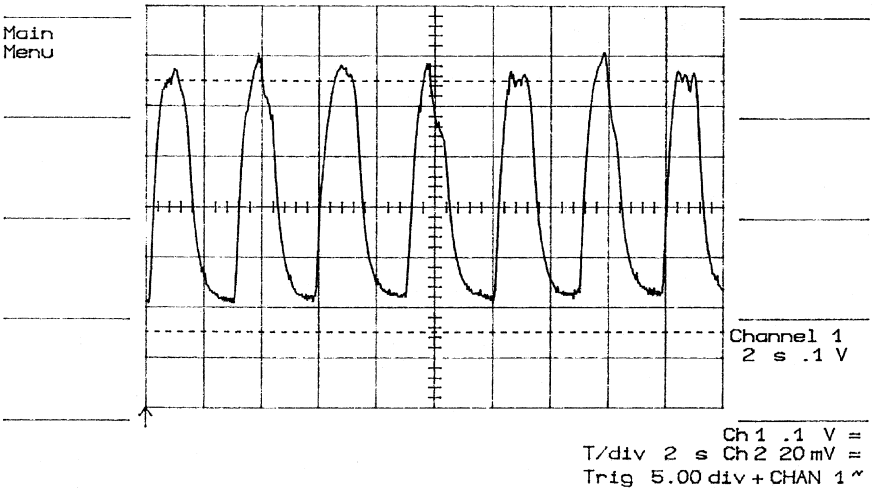

Fig. 4 Response to human breathing of an optical fibre humidity sensor based on a LbL nanoFabry-Perot formed. As indicated in the lower part of the figure, every division along the horizontal axis is 2 s, and every division along the vertical axis is 0.1 V. The materials used were $[Au:PDDA/PSS]_n$. It has been taken from [60]

100 ms, respectively. The main improvement of the sensor proposed here is that the recovery time after an increase of the relative humidity is much shorter than other sensors based on polymeric films.

In Fig. 6 an AFM image gives an idea of the morphology of the film deposited using SiO_2 nanoparticles. In this image the nanoparticle nature of the film is clearly seen and also the roughness of the sensitive coating.

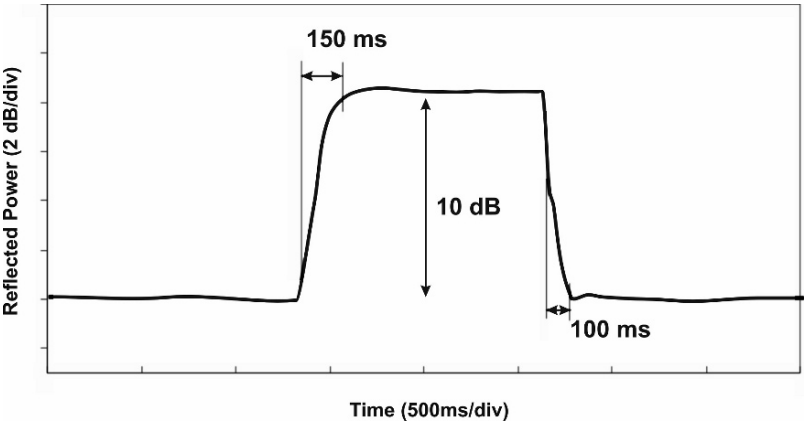

Fig. 5 Dynamic performance of a SiO_2-based optical humidity sensor taken from [61]

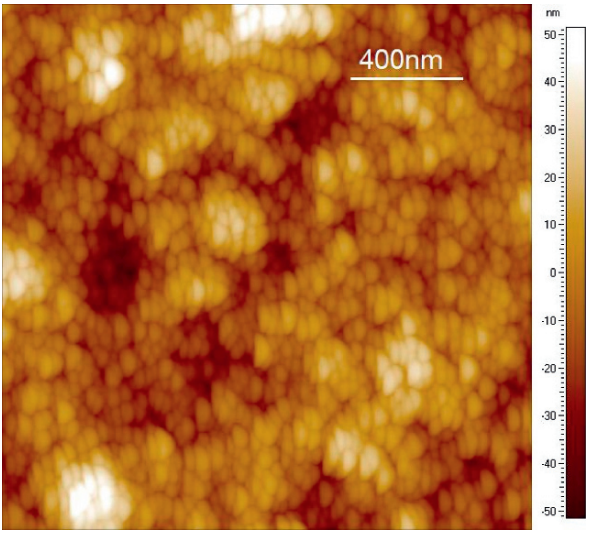

Fig. 6 AFM height image of a film composed by 20 bilayers of 20 nm nanoparticles and 3 bilayers of 7 nm nanoparticles of SiO_2. It has been taken from [61]

3.2 Transmissive Evanescent Wave Sensors

Intrinsic fibre optic humidity sensor can be fabricated using a porous segment of fibre. This can be accomplished using sol gel which when dried has a refractive index similar to that of the fibre. The special segment of fibre can be doped with a humidity sensing material when it is synthesized, for example using $CoCl_2$ [12]. The main drawback of these sensors is the effect of sol gel aging.

On the other hand, a widely employed method to modulate the transmitted power consists of modulating the evanescent wave. The passive cladding of the optical fibre is replaced along a small section by a humidity sensitive material; so any change in the optical or structural characteristic of the chemical dye due to the presence of the humidity, provokes a change in the effective index of the optical fibre, changing its transmission properties [62, 63]. There are several manners to do this; for instance, it is possible to polish the fibre [64] or to use etching with hydrofluoric acid [65]. An easy to implement alternative consists of using plastic cladding fibres (PCS) [66]. In these fibres, the cladding can be removed easily by mechanical methods allowing highly reproducible sensors [67].

The transmittivity is characterized by the refractive index of the dye, the length and the thickness of the new cladding among other parameters. If the new cladding has a lower refractive index than the core the sensor response is governed by the intensity modulation caused by light absorption of the evanescent wave which is guided through the cladding [68]. Otherwise, for higher refractive index, part of the light is refracted into the cladding and part is reflected back to the core [63].

A bent fibre is also an interesting choice to increase the power coupled in the evanescent field and hence the penetration depth in the humidity sensing area [18, 63]. An important part of the light comes out at the curved portion of the fibre, so a bent probe can lead to higher sensitivities in less exposed regions [15].

In the following sections, three structures that use evanescent waves to modulate the transmitted power and whose performance has been studied for nanostructured material are described: tapered optical fibres, hollow core fibres and long period grating fibres.

3.2.1 Tapered Optical Fibres

In this case, the transducer element is a single mode tapered optical fibre coated with a humidity sensitive material. By tapering of the fibre, it is possible to obtain a more fragile but much more sensitive sensor [17].

In the light guided by an optical fibre it can be distinguished two components, the component inside the core, and the evanescent component propagating through the cladding. However, as the cladding is much thicker than the core, the interaction of the exponentially decaying component with the external medium is insignificant. When a single mode fibre is tapered the core/cladding interface is redefined in such a way that the single mode fibre in the central region of the taper (Zone II in Fig. 4) can be seen as a new waveguide formed by the tapered fibre (which acts as the core of the new structure) and the surrounding medium (which acts as the cladding of this waveguide). In consequence, the evanescent field interacts with the outer medium changing the optical power transmitted.

The shape that the fibre acquires after the tapering process, which depends on the method employed in its fabrication, has a high impact on the light transmission properties. The tapering of the fibres can be achieved by heat pulling or chemical etching [69]. Usually chemically etched tapers are characterized by the removal of part of the cladding, while heat pulling tapers maintain the geometrical ratio between cladding and core. Heat pulling tapers can be fabricated using a flame, a laser or an electrical arc. In Fig. 7 a profile of a typical taper is shown. The transition zones have normally different lengths because of the technique used for tapering. As shown in Fig. 7, a tapered fibre can be divided into three regions: a contracting tapered region L_1, a central region (waist) L_c, and an expanding tapered region L_2.

From now on it is supposed a conical distribution taper with step refractive-index profile. Nevertheless, assuming the refractive-index of the optical fibre core as a parabolic distribution, a more realistic theoretical study could be done [70]. Another supposition is that the ratio $S = \rho_{\text{cladding}} / \rho_{\text{core}} = 12.7$ remains constant under tapering and the V-parameter is defined as

$$V_{\text{core}} = \frac{2\pi}{\lambda} \cdot \rho_{\text{core}} \cdot \left(n_{\text{core}}^2 - n_{\text{cladding}}^2 \right)^{\frac{1}{2}} , \tag{5}$$

where λ is the wavelength, ρ_{core} the radius of the core, n_{core} and n_{cladding} are the refractive indices of the core and the cladding respectively. The V-parameter is the

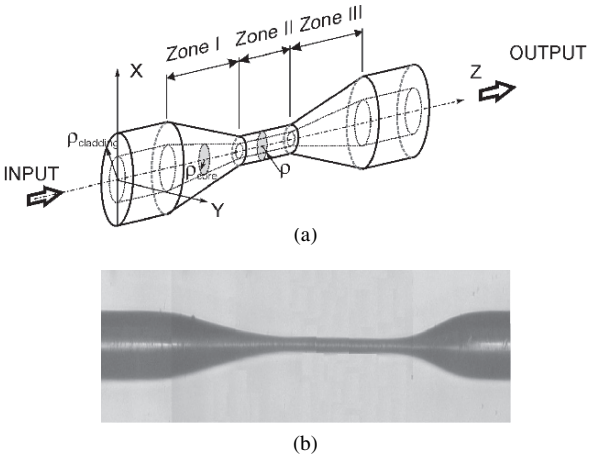

Fig. 7 (**a**) Optical fibre taper profile. (**b**) Photograph of a tapered fibre humidity sensor

normalized frequency of the fibre, a dimensionless parameter, and it gives information about the number of modes propagating in a fibre [71]. When $V = 2.405$ only the lowest order mode is propagating.

Stretching the fibre diameter leads to decrease the value of V, consequently the intensity distribution of the fundamental core mode LP_{01} changes from a narrow profile to a broader one. If V continues decreasing it can reach its cut-off value (V_{cc}) and ρ_{cc} will be the radius of the core when $V = V_{cc}$. This V_{cc} is the minimum value of V to have light guided through the core, for smaller values of V the light cannot be confined in the core. The numerical value of V_{cc} has been determinate as [72]

$$V_{cc} = \sqrt{2/\ln(S)}. \tag{6}$$

From this equation and for typical single-mode fibres with $S \geq 10$ it is predicted $V_{cc} \approx 0.93$. Thus, therefore a good approximation for the following experimental results is to suppose a value of unity for V_{cc} [73].

In other words, for $V = V_{cc}$ the modal field expands and reaches completely the cladding producing a set of cladding modes. Thus, the effect of tapering (for $\rho = \rho_{cc}$) is to create a region where cladding modes exist with a V value much greater that 2.405 [72]. For this reason in a taper we can find a singlemode-multimode transition and a multimode-singlemode transition. This gives us the classical modal domain interferometric structure (singlemode-multimode-singlemode). The coupling mechanism is determined between modes of same angular eigenumbers (LP_{01} to LP_{0x}), mainly between LP_{01} and LP_{02}. It should be remarked that the total optical power (core + cladding) in the taper remains constant [74]. Once the light passes through the waist, the remaining light in the LP_{01} cladding mode is transferred to the LP_{01} core mode which propagates through the conventional optical fibre. The remaining light in other modes gets lost. Theoretical aspects of this phenomenon have been exhaustively studied in [72, 73, 74, 75, 76].

The cladding modes that are the cause of the power loss can be modulated once the tapering process has finished by the deposition of an overlay surrounding material. Small changes in the index of refraction or the thickness of this overlay greatly influence the transmission properties in the multimode central region. The sensitive overlay is used both for creating a humidity sensing surface and for adjusting the working point of the sensor at the point of optimal sensitivity.

As can be seen in the experimental set-up of Fig. 8, the light is coupled from the laser source and is guided until the sensor head, where the light interacts with the humidity sensing material. The signal is transmitted to the optical detector.

In [19, 20, 21, 22] LBL was used to fabricate an optical fibre humidity sensor based on [PDDA/ Poly R-478] nanostructured overlay.

In this work it was shown that the thickness can be controlled in order to optimize the sensor sensitivity, by stopping the deposition process at the maximum slope of the transmitted optical power, achieving 26.8 times better sensitivity with half the thickness.

In Fig. 9(d) the transmittivity of a 20 µm waist diameter taper, coated with the humidity sensitive polymer [PDDA+/Poly-R-] is shown. When the working point is located at a zone of high derivative in the transmission optical power curve, the final sensor was much more sensitive. In Fig. 9(a–c) the experimental response to relative humidity of the three sensors corresponding to the three working points is shown. It is deducted that a higher slope of the transmission characteristic results in sensors with a higher sensitivity. By using the experimental output optical transmission characteristics curve it is possible to find out the maximum slope zone of the

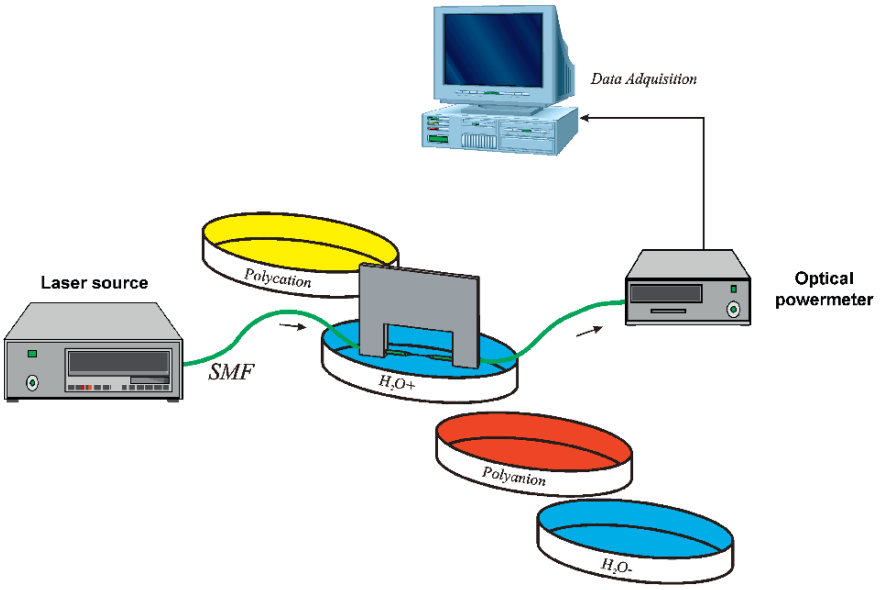

Fig. 8 Transmission set up with a tapered optical fibre based evanescent wave sensor

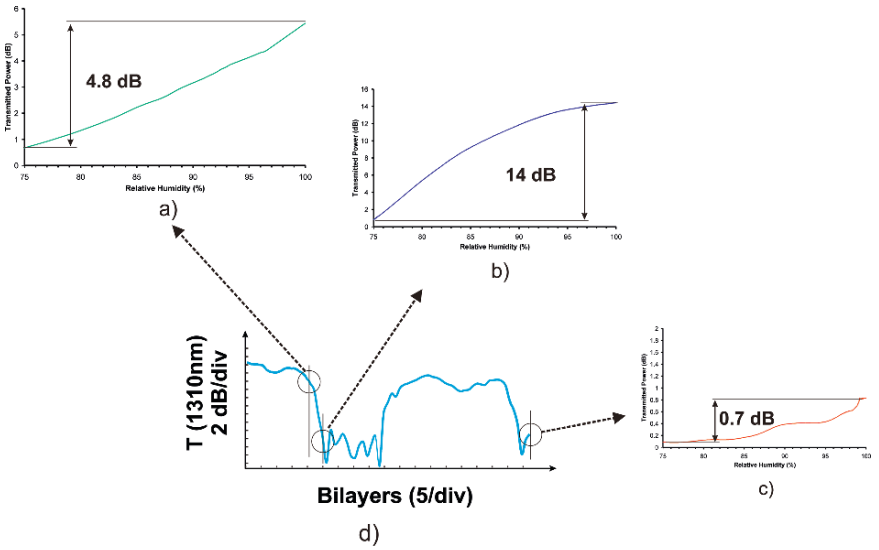

Fig. 9 Experimental response of 20 μm waist diameter TOF based humidity sensors to RH corresponding to three working points of coating thicknesses: (**a**) 23 bilayers, (**b**) 26 bilayers and (**c**) 62 bilayers. (**d**) Transmitivity as a function of the sensitive deposited nano-film thickness. Taper length: 2.2 mm. Nano-film: [PDDA+/Poly-R-]. λ = 1310 nm [19]

potential sensor in order to fabricate an optimized sensitivity sensor with a coating thickness tuned around this working point.

3.2.2 Hollow Core Fibres

Another possibility for increasing the amount of optical power coupled in the evanescent field is by using new types of fibres that have appeared a few years ago. Among then, one can mention hollow core fibres. The simpler type of hollow core fibres, consist basically of tubular fibres where the optical signal is guided mainly by the cladding, and hence, it is easy to reach the evanescent fields. If a short portion of a hollow core fibre is spliced spliced to a multimode fibre (MMF) using the appropriate electric arc conditions, the HCF collapses, forming a tapered solid fibre in the interface between both fibres (see Fig. 10). In these devices, the light that is guided in the core of a lead-in MMF can be coupled to the cladding of the HCF due to the tapered region instead of being confined in the air core. When the light reaches the lead-out MMF, it is coupled into the silica core again. Because the light is guided by the silica cladding in the HCF region, these devices, called MHM, can be used as evanescent field sensors that are sensitive to any coating deposited onto this region and have been also used to build optical fibre humidity sensors in [22, 23, 24].

In order to understand the influence of some important parameters on the behavior of the MHM, in this and case in contrast to the previous architecture, a ray model

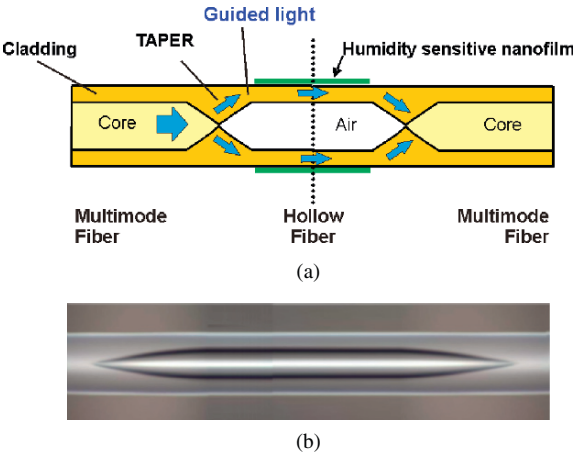

Fig. 10 (**a**) Hollow core fibre with microstructurated cladding, connected between two standard multimode optical fibre sections. A sensitive material can be also fixed onto the cladding. (b) Photograph of a MHM sensor

for a one-dimensional waveguide is developed (see Fig. 11). This model calculates the transmitted power in the HCF after the multiple reflections of light at the interface between the HCF and the exterior. The light source is assumed to be a lambertian one oriented in the direction of propagation of the waveguide. The transmitted power when no deposition has been performed on the HCF will be taken as a reference value (0 dB). This one-dimensional simple model is enough to qualitatively

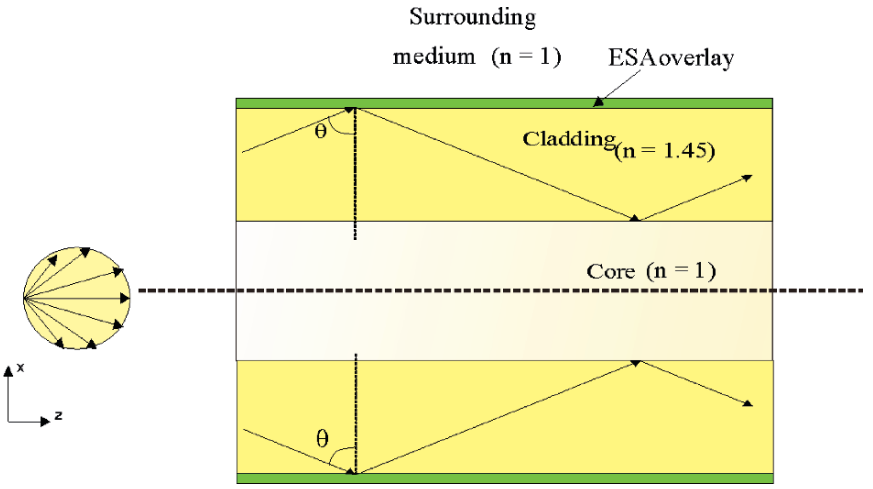

Fig. 11 Theoretical model: a lambertian light source impinges on a one-dimensional slab waveguide with an LBL overlay on one side

demonstrate the behavior of the structure. If more accuracy is required, a more complex two-dimensional model is necessary.

Working with evanescent field sensors one important characteristic of the material deposited is the refractive index. In this work it has been only deposited [PDDA/Poly R], which refractive index is higher than that of the fibre. In order to know what response the devices will have with different refractive index coatings some simulations were done. The simulations were done with three different refractive indexes, the one obtained in the experiments, another lower and the other one higher; exactly $1.54 + 0.004i$, $1.37 + 0074i$ and $1.67 + 0.004i$, respectively. The length of the HCF section used for the simulations was 20 mm and the wavelength of the light source was 1310 nm. The results are shown in Fig. 12.

The response of the device is very different when the refractive index changes. The transmitted optical power of the devices when $n = 1.65$ and $n = 1.54$ falls oscillatory as the thickness of the material deposited is increased unlike the power of the device when $n = 1.37$ which has no oscillations. As can be seen, the depth and period of the theoretical curve are bigger when $n = 1.54$ than when $n = 1.65$. On the other hand, although the fall of the theoretical curve for $n = 1.37$ is not the biggest one, since its transmission slope in the first few nanometers of thickness is very high it could be used to develop very sensitive sensors, depositing materials with the appropriate refractive index and with a thickness of few decades of nanometers.

Some experimental results are presented in Fig. 13; the HCF segment used in the MHM has a length of 20 mm, and diameters of 50/150 µm.

The power transmitted by MHM structures follows an oscillatory way as the number of nano-bilayers deposited gets increased. As it can be seen, the period of this oscillation depends, among other parameters, on the wavelength of the light source as expected due to the modal interferometer behaviour it exhibits. Furthermore, it is observed a gradual decrease of transmission due to the non-zero

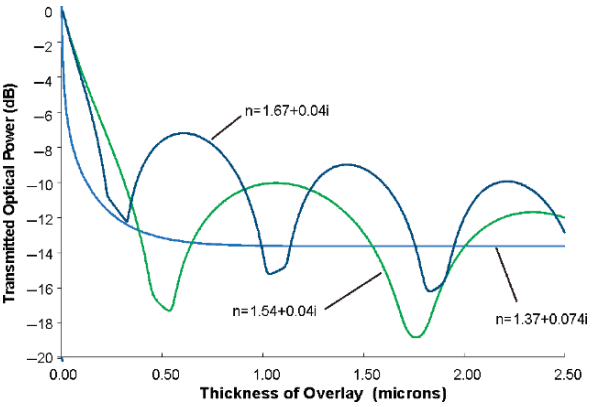

Fig. 12 Theoretical optical power transmitted by three MHM devices 20 mm long when the refractive index of the material deposited are: $1.54 + 0.004i$, $1.37 + 0074i$ and $1.67 + 0.004i$ at 1310 nm. Waveguide thickness: 50 microns [23]

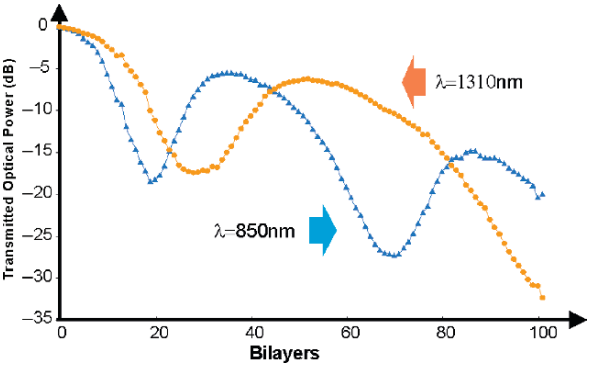

Fig. 13 Experimental data of the optical power transmitted by one MHM device 20 mm long with HCF 50/150 µm inner and outer diameters at two different wavelength: 850 nm and 1310 nm [23]

imaginary part of the refractive index of the nano-film deposited. The amplitude of the oscillatory behaviour of the transmitted power trends to reduce when the inner diameter decreases because the evanescent field ratio respect to the total transmitted optical power is higher. There exists others parameters that also affect to the optical power transmission of this device as the length of the HCF section, the splice machine parameters used to tapered the multimode fibres (that is, the slope of the taper) the index of refraction of the overlay, etc.

Also, to evaluate the response of these proposed sensors, we exposed the sensor head to rapid changes of the RH. Human breathing contains more water vapour than the normal room environment. Accordingly, the sensor was set 3 cm from a subject's mouth. The results obtained are shown in Fig. 14. The observed rise response times were around 300 ms. The fall times were less than a couple of seconds.

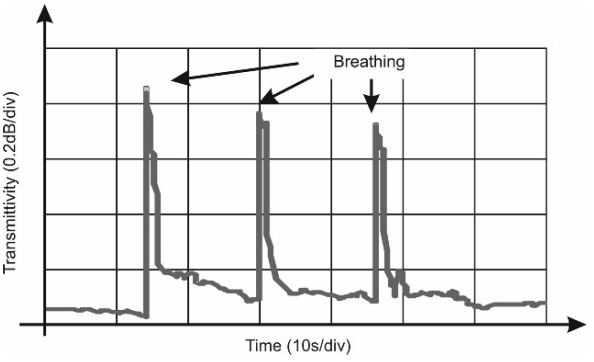

Fig. 14 Experimental response to human breathing using a 20 mm-long HCF. Taken from [77]

3.2.3 Long Period Fibre Bragg Grating

Long Period Fibre Gratings (LPFGs) are based on a periodic index modulation of the refractive index of the core of a single mode fibre (SMF), with a period between 100 microns and 1 mm. LPFGs induce attenuation bands in the transmission spectrum based on the coupling between the core mode and the copropagating cladding modes. Because of that, the influence of the surrounding medium on the LPFGs transmission is more important than in fibre Bragg gratings (FBGs), where there is a contrapropagative coupling only between core modes. It has been experimentally proved that the deposition of thin layers onto the surface of the fibre using Langmuir Blodgett (LB) technique, LBL or dip-coating, can induce important changes in the resonance wavelengths [78, 79, 80, 81, 82, 83, 84, 85]. In this way, long-period fibre gratings (LPFGs) can used for the construction of evanescent wave sensor; the changes of the deposited overlay due to the humidity induce changes in position of the attenuation bands that are collected in the OSA.

In Fig. 15 it is represented the typical setup used for monitorization of the transmission spectra in a long-period fibre grating (LPFG). The flat spectrum from a broadband source is launched into the optical fibre and at the output, the transmission spectrum with the attenuation bands generated due to the coupling of light from the core mode to the cladding modes, is collected in an optical spectrum analyzer (OSA).

There are two key points that define each attenuation band. The first one is its depth. This can be approximated with this expression [86]:

$$T_i = \cos^2(k_i L) \tag{7}$$

where i is the cladding mode order, k_i is the coupling coefficient and L the length of the grating.

The second key point is the resonance wavelength. Though the simple phase matching condition is sufficient to give an approximation of the central wavelength of the attenuation band, the modified phase matching condition is often preferred [87] :

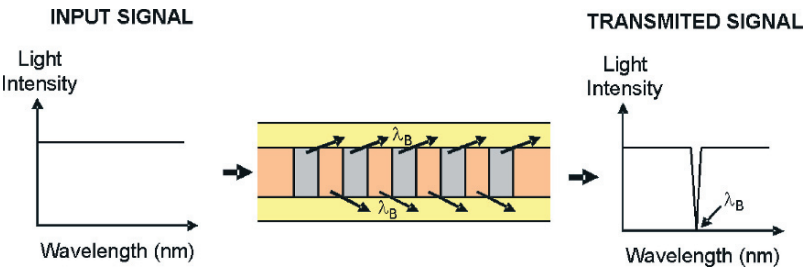

Fig. 15 Schematic working principles of LPFG

$$\beta_{01}(\lambda) + s_0\zeta_{01,01}(\lambda) - \left(\beta_{0j}(\lambda) + s_0\zeta_{0j,0j}(\lambda)\right) = \frac{2\pi N}{\Lambda} \tag{8}$$

where β_{01} and β_{0j} are the propagation constants of the core and the j cladding modes respectively, $\varsigma_{01,01}$ and $\varsigma_{0j,0j}$ are the self-coupling coefficients of the core and the j cladding modes, s_0 is the coefficient of the zero-frequency Fourier component of the grating, Λ is the period of the grating, and N is the diffraction order.

The development of numerical methods has helped to understand the phenomena involved in these experiments. The wavelength shift of the attenuation bands was explained in [88] with a scalar analysis of modes (LP mode approximation) and the application of coupled mode theory [87]. If an overlay of higher refractive index than the cladding is deposited on this LPFG, as the overlay thickness increases, cladding modes shift their effective index to higher values. When the overlay is thick enough, one of the cladding modes is guided by the overlay. This causes a reorganization of the effective index of the rest of modes.

In Fig. 16 the effective index of the first ten cladding modes are represented as a function of the coating thickness. The notation used is $LP_{0,2}$ for the first cladding mode, $LP_{0,3}$ for the second cladding mode and so on. Cladding modes with lower effective index than the one that is guided by the overlay will shift their effective index value towards the effective index of the immediate higher effective index mode.

As more material is deposited, the effective index distribution before deposition is recovered. The effective index of the eighth cladding mode will be now that of the seventh one, the effective index of the seventh cladding mode will be that of the sixth mode, and so on. During the first redistribution there is a sudden effective index increase for the $LP_{0,2}$ mode. The same is true for the $LP_{0,3}$ mode during the second redistribution, for the $LP_{0,4}$ in the third one, and for the $LP_{0,5}$ in the fourth one. A more detailed explanation of these statements can be found in [88].

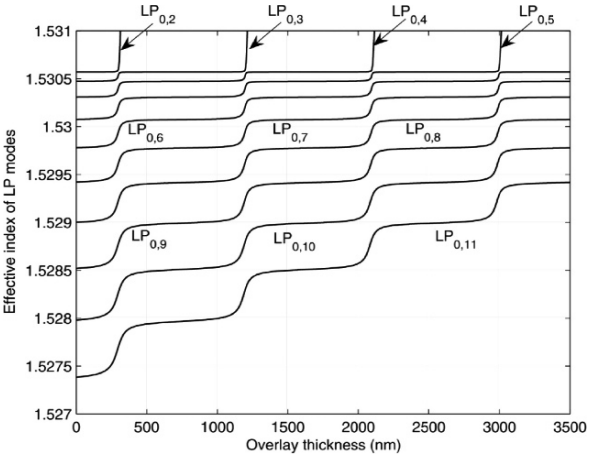

Fig. 16 Effective index of the first ten cladding modes as a function of the overlay thickness of the nano-film deposited

The same phenomenon observed for the effective index of the modes is true for the resonance wavelength values because there is a close relation between the resonance wavelength of each attenuation band and the effective index of its corresponding cladding mode.

Several studies have been developed in the last years related to the experimental behaviour of the LPFG to thin layers [25, 78, 79, 80, 81, 82, 83, 84, 85, 89]. When an intermediate external medium (a coating) is added between the surrounding medium and the cladding of the LPFG two additional parameters are added: the overlay refractive index and the overlay thickness which can be controlled using the appropriate deposition technique. By adequate parameterization of the overlay thickness and overlay refractive index the device can be optimized for a maximum wavelength shift, thus a maximum sensitivity, as a function of specific parameters [90, 91]. An usually employed method for improving the sensitivity is based on the deposition of a thin overlay on the cladding of an LPFG. In this way, it is possible to design a device with optimal sensitivity. The phenomenon has also been experimentally analyzed with an improvement in the sensitivity of the device by more than ten times [85].

In [92] a humidity sensor using a long-period fibre grating (LPG) and a SiO_2-nanospheres coating was developed. Figure 17 shows a humidity cycle. The dashed line represents the relative humidity variation, and the straight line represents the peak of absorption of the LPG. At different humidity values, the polymeric overlay changes its optical properties yielding to a shift in the resonance wavelength of the LPG. Wavelength shifts up to 12 nm in a range from 20 to 80% of humidity level were obtained. When the relative humidity increases, the resonance wavelength peak shifts to lowers wavelengths. This effect is due to changes accomplished in the refractive index of the SiO_2-nanospheres film.

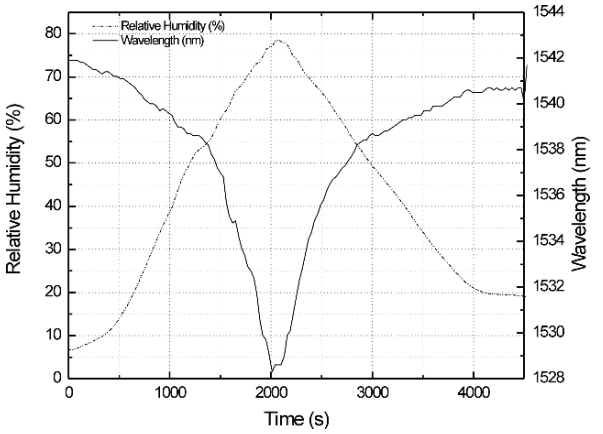

Fig. 17 Resonance wavelength shift for different relative humidity levels. It has been taken from [94]

4 Conclusions

The field of optical fibre humidity sensors has been reviewed, with special attention to those coated with nanostructured films. The basics of the LBL method applied to the fabrication of humidity sensitive coatings have been described. The main sensing mechanisms and architectures have been studied paying attention to the different methods of fabrication; both reflection and transmission configurations have been taken into account. The first one is based on the deposition on the tip of optical fibre creating a nanocavity, while the second group is based mainly on evanescent field based modulation.

Acknowledgments This work was funded in part by the Spanish Ministry of Education and Science – FEDER TEC2006-12170/MIC Research Grant and Government of Navarra-Feder Euroinnova Research Grants.

References

1. Fuhr, P.L.; Huston, D.R., Corrosion detection in reinforced concrete roadways and bridges via embedded fibre optic sensors. In: Smart Mater. Struct., 1998, 7, 217–228.
2. Cooper, K.R.; Elster, J.; Jones, M.; Kelly, R.G., Optical fibre-based corrosion sensor systems for health monitoring of aging aircraft, In: Autotestcon Proceedings, IEEE Systems Readiness Technology Conference, Aug. 2001, 847–856, 20–23.
3. Bownass, D.C.; Barton, J.S.; Jones, J.D.C., Detection of high humidity by optical fibre sensing at telecommunications wavelengths, Optics Communications, 15 January 1998, 146 (1), 90–94(5).
4. Mc Murtry, S.; Wright, J.D.; Jackson, D.A., Sensing applications of a low-coherence fibre-optic interferometer measuring the refractive index of air, Sensors and Actuators B: Chemical, 5 January 2001, 72 (1), 69–74.
5. Matsumoto, S., New air density and absolute humidity sensors using optical fibre cable and alpha-rays, Meas. Sci. Technol. 2001, 12, 865–870.
6. McMurtry, S.; Wright, J.D.; Jackson, D. A., A multiplexed low coherence interferometric system for humidity sensing, Sensors and Actuators B, 2000, 67, 52–56.
7. Brook, T.E.; Narayanaswamy, R., Polymeric films in optical gas sensors, Sensors and Actuators, B: Chemical, 1998, 51(1–3), 77–83.
8. Raimundo, I.M., Jr. Narayanaswamy, R., Evaluation of Nafion-Crystal Violet films for the construction of an optical relative humidity sensor, Analyst, 1999, 124(11), 1623–1627.
9. Corera, F. P.; Gaston A.; Sevilla, J.; Relative humidity sensor based on side-polished fibre optic, Proceedings of the 17th IEEE Instrumentation and Measurement Technology Conference, 2000. IMTC 2000.
10. Ballantine, D.S.; Wohltjen, H., Optical waveguide humidity detector, Analytical Chemistry, 1986, 58(13), 2883–2885.
11. Russel, A.P.; Fletcher, K.S., Optical sensor for the determination of moisture, Anal. Chim. Acta 1985, 170, 209–216.
12. Zhou, Q.; Shahriari, M.R.; Kritz, D.; Sigel G.H. Jr., Porous fibre optic sensor for high sensitivity humidity measurements, Anal. Chem. 1988, 60, 2317–2320.
13. Boltinghouse, F.; Abel, K. Development of an optical relative humidity sensor. Cobalt chloride optical absorbency sensor study, Analytical Chemistry, 1989, 61(17), 1863–1866.

14. Choi, M.M.F.; Ling, T.O., Humidity-sensitive optode membrane based on a fluorescent dye immobilized in gelatin film, Analytica Chimica Acta, 1999, 378(1–3), 127–134.
15. Otsuki, S.; Adachi, K.; Taguchi T., A novel fibre-optic gas-sensing configuration using extremely curved optical fibres and an attempt for optical humidity detection, Sensors and Actuators, B: Chemical, 1998, 53(1–2), 91–96.
16. Campo, J.C.; Perez, M.A.; Gonzalez, M.; Ferrero, F.J., Measurement of air moisture by the phosphorescence lifetime of a sol-gel based sensor, Proceedings of the 17th IEEE Instrumentation and Measurement Technology Conference, 2000. IMTC 2000, 1, 273–276.
17. Bariain, C.; Matias, I.R.; Arregui, F.J.; Lopez-Amo, M., Optical fibre humidity sensor based on a tapered fibre coated with agarose gel, Sensors and Actuators B, 2000, 69, 127–131.
18. Gupta, B.D.; Ratnanjali, A novel probe for a fibre optic humidity sensor, Sensors and Actuators B: Chemical, 20 November 2001, 80 (2), 132–135(4).
19. Corres, J.M.; Arregui, F.J.; Matias, I.R., Sensitivity optimization of tapered optical fibre humidity sensors by means of tuning the thickness of nanostructured sensitive coatings, Sensors and Actuators, B: Chemical, 2007, 122(2), 442–449.
20. Corres, J.M.; Bravo, J.; Matias, I.R.; Arregui, F.J., Nonadiabatic tapered single-mode fibre coated with humidity sensitive nano-films, IEEE Photonics Technology Letters, 2006, 18(8), 935–937.
21. Corres, J.M.; Arregui, F.J.; Matias, I.R., Design of humidity sensors based on tapered optical fibres, Journal of Lightwave Technology, 2006, 24(11), 4329–4336.
22. Matias, I.R.; Arregui, F.J.; Corres, J.M.; Bravo, J., Evanescent field fibre-optic sensors for humidity monitoring based on nanocoatings, IEEE Sensors Journal, 7(1), 89–95.
23. Bravo, J.; Matias, I.R.; Del Villar, I.; Corres, J.M.; Arregui, F.J., Nano-films on hollow core fibre-based structures: An optical study, Journal of Lightwave Technology, 2006, 24(5), 2100–2107.
24. Matias, I.R.; Bravo, J.; Arregui, F.J.; Corres, J.M., Nano-films on a hollow core fibre, Optical Engineering, 2006, 45(5), Art. No. 050503.
25. Del Villar, I.; Corres, J.M.; Achaerandio, M.; Arregui, F.J.; Matias, I.R., Spectral evolution with incremental nanocoating of long period fibre gratings, Optics Express, 2006, 14(25), 11972–11981.
26. Jindal, R.; Tao, S.; Singh, J.P.; Gaikwad, P.S., High dynamic range fibre optic relative humidity sensor, Opt. Eng., May 2002, 41(5), 1093–1096.
27. Iler, R.J.J. Multilayers of colloidal particles, Journal of Colloid and Interface Science, June 1966, 21 (6), 569–594.
28. Decher, G.; Fuzzy Nanoassemblies: Toward Layered Polymeric Multicomposites, Science, 1997, 277: 1232–1237.
29. Lvov, Y., Ariga, K., Ichinose, I., Kunitake, T., Assembly of multicomponent protein films by means of electrostatic layer-by-layer adsorption, J. Am. Chem. Soc., 1995, 117(22), 6117–6123.
30. Ariga, K.; Lvov, Y.; Kunitake, T., Assembling alternate dye-polyion molecular films by electrostatic layer-by-layer adsorption, J. Am. Chem. Soc., 1997, 119(9), 2224–2231.
31. Liu, Y.; Wang, A.; Claus, R., Molecular self-assembly of TiO2/polymer nanocomposite films, J. Phys. Chem. B., (Article), 1997, 101(8), 1385–1388.
32. Liu, Y.J.; Wang, A.B.; Claus, R.O., Layer-by-layer electrostatic self-assembly of nanoscale Fe3O4 particles and polyimide precursor on silicon and silica surfaces. Appl. Phys. Lett., 1997, 71, 2265–2267.
33. Liu, Y.J.; Wang, A.B.; Claus, R.O., Layer-by-layer ionic self-assembly of Au colloids into multilayer thin-films with bulk metal conductivity, Chem. Phys. Lett., 1998, 298, 315–319.
34. Lenahan, K. M.; Wang, A. B.; Liu, Y. J.; Claus, R. O., Novel polymer dyes for nonlinear optical applications using ionic self-assembled monolayer technology. Adv. Mater. 1998, 10, 853–855.
35. Donath, E.; Sukhorukov, G. B.; Caruso, F.; Davis, S.A.; Mohwald, H., Novel hollow polymer shells by colloid-templated assembly of polyelectrolytes. Angewandte Chemie-International Edition, 1998, 37, 2202–2205.

36. Caruso, F.; Caruso, R. A.; Mohwald, H., Nanoengineering of inorganic and hybrid hollow spheres by colloidal templating, Science, 1998, 282, 1111–1114.
37. Caruso, F.; Lichtenfeld, H.; Donath, E.; Mohwald, H., Investigation of electrostatic interactions in polyelectrolyte multilayer films: binding of anionic fluorescent probes to lLayers assembled onto colloids, Macromolecules, 1999, 32, 2317–2328.
38. Chen, L. H.; McBranch, D. W.; Wang, H. L.; Helgeson, R.; Wudl, F.; Whitten, D. G., Highly sensitive biological and chemical sensors based on reversible fluorescence quenching in a conjugated polymer, Proceedings of the National Academy of Sciences of the United States of America, 1999, 96, 12287.
39. Dubas, S. T.; Schlenoff, J. B., Factors controlling the growth of polyelectrolyte multilayers, Macromolecules, 1999, 32, 8153–8160.
40. Mamedov, A. A.; Kotov, N. A.; Prato, M.; Guldi, D. M.; Wicksted, J. P.; Hirsch, A., Molecular design of strong single-wall carbon nanotube/polyelectrolyte multilayer composites, Nature Materials 2002, 1, 190.
41. Nakagawa, M.; Oh, S. K.; Ichimura, K., Photopatterning and visualization of adsorbed monolayers of bis(l-benzyl-4-pyridinio)elhylene moieties, Adv. Mater., 2000, 12, 403–407.
42. Ho, P.K.H.; Kim, J.S.; Burroughes, J.H.; Becker, H.; Li, S.F.Y.; Brown, T.M.; Cacialli, F.; Friend, R.H., Molecular-scale interface engineering for polymer light-emitting diodes, Nature, 2000, 404 (6777), 481–484.
43. Shiratori, S. S.; Rubner, M. F., pH-dependent thickness behavior of sequentially adsorbed layers of weak polyelectrolytes, Macromolecules, 2000, 33, 4213–4219.
44. Bertrand, P.; Jonas, A.; Laschewsky, A.; Legras R., Ultrathin polymer coatings by complexation of polyelectrolytes at interfaces: Suitable materials, structure and properties, Macromolecular Rapid Communications, 2000, 21, 319–348.
45. Mendelsohn, J.D.; Barret, C.J.; Chan, V.V.; Pal, A.J.; Mayes, A.M.; Rubner, M.F., Fabrication of microporous thin films from polyelectrolyte multilayers, Langmuir, 2000, 16, 5017–5023.
46. Mattoussi, H.; Mauro, J.M.; Goldman, E.R.; Anderson, G.P.; Sundar, V.C.; Mikulec, F.V.; Bawendi, M.G., Self-assembly of CdSe-ZnS quantum dot bioconjugates using an engineered recombinant protein, J. Am. Chem. Soc. 2000, 122, 12142–12150.
47. Schreiber, F., Structure and growth of self-assembling monolayers, Progress in Surface Science, 2000, 62, 151–256.
48. Caruso, F., Nanoengineering of particle surfaces, Adv. Mater. 2001, 122, 11–22.
49. Adams, D.M.; Brus, L.; Chidsey C.E.D.; Creager, S.; Creutz, C.; Kagan, C.R.; Kamat, P.V.; Lieberman, M.; Lindsay, S.; Marcus, R.A.; Metzger, R.M.; Michel-Beyerle, M.E.; Miller, J.R.; Newton, M.D.; Rolison, D.R.; Sankey, O.; Schanze, K.S.; Yardley, J.; Zhu, X.Y., Charge transfer on the nanoscale: Current status, J. Phys. Chem. B, 2003, 107, 6668–6697.
50. Schönhoff, M., Self-assembled polyelectrolyte multilayers, Current Opinion in Coll. Interf. Sci. 2003, 8, 86.
51. Thünemann, A.F.; Müller, M.; Dautzenberg, H.; Joanny, J.-F.; Löwen, H., Polyelectrolyte Complexes, Advances in Polymer Science 2004, 166, 113–171.
52. Hammond, P.T., Form and function in multilayer assembly: New applications at the nanoscale, Adv. Mater. 2004, 16, 1271–1293.
53. Choi, J.; Rubner, M.F., Influence of the degree of ionization on weak polyelectrolyte multilayer assembly, Macromolecules, 2005, 38, 116–124.
54. Del Villar, I.; Matias, I.R.; Arregui, F.J., LBL-based in-fibre nanocavity for hydrogen-peroxide detection, IEEE Trans. on Nanotech. 2005, 4, 187–193.
55. Hu, W.; Liu, Y.; Xu, Y.; Liu, S.; Zhou, S.; Zeng, P.; Zhu, D.B., The gas sensitivity of Langmuir-Blodgett films of a new asymmetrically substituted phthalocyanine. Sensor. Actuat. B-Chem., 1999, 56, 228–233.
56. Bariain, C.; Matias, I.R.; Fernandez-Valdivielso, C.; Arregui, F.J.; Rodríguez-Méndez, M.L.; DLbLja, J.A., Optical fibre sensor based on lutetium bisphthalocyanine for the detection of gases using standard telecommunication wavelengths. Sensor. Actuat. B-Chem., 2003, 93, 153–158.

57. Gutierrez, N.; Rodríguez-Méndez, M.L.; De Saja, J.A., Array of sensors based on lanthanide bisphthalocyanine Langmuir-Blodgett films for the detection of olive oil aroma. Sensor. Actuat. B-Chem. 2001, 77, 437–442.
58. Dakin, J.; Culshaw, B., Optical fibre sensors. Principles and components, Norwood, MA: Artech House. 1988, pp. 63–64.
59. Arregui, F.J.; Matias, I.R.; Liu, Y.J.; Lenahan, K.M.; Claus, R.O., Optical fibre nanometer-scale Fabry-Perot interferometer formed by the ionic self-assembly monolayer process, Opt Lett., 1999, 24, 596–598.
60. Arregui, F.J.; Liu, Y.; Matias, I.R.; Claus, R.O.; Optical fibre humidity sensor using a nano Fabry–Perot cavity formed by the ionic self-assembly method, Sensors and Actuators B 59 1999.54–59
61. Corres, J. M.; Matias, I. R.; Hernaez, M.; Bravo, J.; Arregui, F. J., Optical fibre humidity sensors using nanostructured coatings of SiO2 nanoparticles, IEEE Sensors Journal, Vol. 8, Issue 3, March 2008, pp. 281–285.
62. Khalil, S.; Bansal, L.; El-Sherif, M., Intrinsic fibre optic chemical sensor for the detection of dimethyl methylphosphonate. Opt. Eng., 2004, 43, 2683–2688.
63. Otsuki, S.; Adachi, K.; Taguchi, T.; A novel fibre-optic gas-sensing configuration using extremely curved optical fibres and an attempt for optical humidity detection, Sensors and Actuators B, 1998, 53, 91–96.
64. Senosiain, J.; Díaz, I.; Gastón, A.; Sevilla, J., High sensitivity temperature sensor based on side-polished optical fibre. IEEE Trans. Instrum. Meas. 2001, 50, 1656–1660.
65. Sumdia, S.; Okazaki, S.; Asakura, S.; Nakagawa, H.; Murayama, H.; Hasegawa, T., Distributed hydrogen determination with fibre-optic sensor. Sensor. Actuat. B-Chem. 2005, 108, 508–514.
66. Cherif, K.; Mrazek, J.; Hleli, S.; Matejec, V.; Abdelghani, A.; Chomat, M.; Jaffrezic-Renault, N.; Kasik, I., Detection of aromatic hydrocarbons in air and water by using xerogel layers coated on PCS fibres excited by an inclined collimated beam. Sensor. Actuat. B-Chem., 2003, 95, 97–106.
67. Suzuki, O.; Miura, M.; Morisawa, M.; Muto, S., POF-type optic humidity sensor and its application (as breathing-condition monitor), in: Proceedings of the 15th Optical Fibre Sensors Conference (OFS 2002), Technical Digest, Orlando, OR, 2002, pp. 447–450.
68. Yuan, J.; El-Sherif, A. Fibre-optic chemical sensor using polyaniline as modified cladding material. IEEE Sensor. J. 2003, 3, 5–12.
69. Haddock, H.S.; Shankar, P. M.; Mutharasan, R., Fabrication of biconical tapered optical fibres using hydrofluoric acid. Materials science and engineering B, 2003, 97, 87–93.
70. Yuan, L.; Qui, A., Analysis of a single-mode fibre with taper lens end, J. Opt. Soc. Am. A, 1992, 9, 950–952.
71. Senior, J.M., Optical fibre communications. Principles and practice, Prentice Hall, Hertfordshire, 2nd edn., 1992, pp. 40–58.
72. Black, R.J.; Bourbonnais, R., Core-mode cutoff for finite-cladding lightguides, IEE Proceedings-J., 133 1986, (6), 277–384.
73. Love, J.D.; Henry, W.M.; Stewart, W.J.; Black, R.J.; Lacroix, S.; Gonthier, F., Tapered single-mode fibres and devices. Part 1: Adiabatic criteria, IEE Proceedings-J, 1991, 138(5), 343–353.
74. Bobb, L.C.; Shankar, P.M.; Krumboltz, H.D., Bending effects in biconically tapered single-mode fibres, J. Light. and Tech. 1990, 8, 1084–1090
75. Birks, T. A.; Russell, P.; St. and Pannel, C. N.; Low power acousto-optic device based on a tapered single mode fibre, IEEE Phot. Tech. Let. 1994, 6 725–727.
76. Shankar, P.M.; Bobb, L. C.; Krumboltz, H.D.; Coupling of modes in bent biconically tapered single-mode fibres, J. of Light. Techn., 1991, 9(7), 832–837.
77. Matías, I.R.; Corres, J. M.; Arregui, F. J.; Bravo, J., Humidity sensors using nano-films deposited on hollow core fibres, SPIE Newsroom, International Society for Optical Engineering.
78. Rees, N. D.; James, S. W.; Tatam, R. P.; Ashwell, G. J., Optical fibre long-period gratings with Langmuir-Blodgett thin-film overlays, Opt. Lett., 2002, 27, 686–688.

79. Del Villar, I.; Achaerandio, M.; Matias, I. R.; Arregui, F. J., Deposition of overlays by electrostatic self-assembly in long-period fibre gratings, Opt. Lett., 2005, 30, 720–722.
80. Wang, Z. Y.; Heflin, J. R.; Stolen, R. H.; Ramachandran, S., Analysis of optical response of long period fibre gratings to nm-thick thin-film coatings, Opt. Exp., 2005, 13, 2808–2813.
81. Kim, D.W.; Zhang, Y.; Cooper, K.L.; Wang, A., In-fibre reflection mode interferometer based on a long-period grating for external refractive-index measurement, App. Opt., 2006, 44, 5368.
82. Chen, Q.; Lee, J.; Lin, M.R.; Wang, Y.; Yin, S.S.; Zhang, Q.M.; Reichard, K.A., Investigation of tuning characteristics of electrically tunable long-period gratings with a precise four-layer model, J. Lightwave Technol., 2006, 24, 2954–2962.
83. Cusano, A.; Iadicicco, A.; Pilla, P.; Contessa, L.; Campopiano, S.; Cutolo, A.; Giordano, M., Cladding mode reorganization in high-refractive-index-coated long-period gratings: Effects on the refractive-index sensitivity, Opt. Lett., 2005, 30, 2536–2538.
84. Pilla, P.; Iadicicco, A.; Contessa, L.; Campopiano, S.; Cutolo, A.; Giordano, M.; Cusano, A., Optical chemo-sensor based on long period gratings coated with δ form syndiotactic polystyrene, IEEE Photon. Technol. Lett., 2005, 17, 1713–1715.
85. Cusano, A.; Iadicicco, A.; Pilla, P.; Contessa, L.; Campopiano, S.; Cutolo, A.; Giordano, M., Mode transition in high refractive index coated long period gratings, Opt. Express, 2006, 14, 19–34.
86. Erdogan, T.; Fibre grating spectra, J. Lightwave Technol., 1997, 15, 1277–1294.
87. Anemogiannis, E.; Glytsis E. N.; Gaylord, T. K., Transmission characteristics of long-period fibre gratings having arbitrary azimuthal/radial refractive index variations, J. Lightwave Technol., 2003, 21, 218–227.
88. Del Villar, I.; Matias, I. R.; Arregui, F. J.; Lalanne, P., Optimization of sensitivity in long period fibre gratings with overlay deposition, Opt. Express, 2005, 13, 56–69.
89. Del Villar, I.; Matias, I.R.; Arregui, F.J.; Achaerandio, M., Nanodeposition of materials with complex refractive index in long-period fibre gratings, Journal of Lightwave Technology, 2005, 23(12), 4192–4199.
90. Chung, K.W.; Yin, S., Analysis of a widely tunable long-period grating by use of an ultrathin cladding layer and higher-order cladding mode coupling, Opt. Lett., 2004, 29, 812–814.
91. Lyons, E.R.; Lee, H.P., Demonstration of an etched cladding fibre Bragg grating filter with reduced tuning force requirement, IEEE Photon. Technol. Lett., 1999, 11, 1626–1628.
92. Viegas, D.; Goicoechea, J.; Corres, J.M.; Matias, I.R.; Araújo, F.M.; Santos, J.L., Humidity sensing based on SiO_2-nanospheres onto a Long-Period Fibre Grating, OFS-2008 Optical Fibre Sensors International Conference.